A METHOD FOR IMPROVING THE RESOLUTION OF MULTIPLE SIGNALS IN PERIODIC FOURIER TRANSFORM

Xiangcheng CHEN[1], Jiandong ZHU[2,*], Lijuan QIAO[3]

The periodic fractional Fourier transform (PFRFT) is very suitable for estimating linear frequency modulated continuous wave (LFMCW) signals. The resolution problem of multi-component LFMCW signals in the periodic fractional domain is studied in this article. Firstly, the article provides a detailed mathematical derivation and analysis of the spectrum features and critical resolution distance between multiple signal spectra under the condition of discrete PFRFT calculation. It is concluded that discrete scaling and dimensional normalization processing can improve the peak distance between multiple signals. Then, it proposes a comprehensive optimization method for selecting Dimensional normalization factors to enhance the resolution of PFRFT for multiple LFMCW signals. Finally, the method is validated using simulation signals.

Keywords: Multi-signal resolution; normalization of dimensional scales; periodic fractional Fourier transform; spectral characteristics

1. Introduction

The fractional Fourier transform (FRFT) [1] is a generalized form of the Fourier transform and can be understood as a linear frequency modulation (LFM) basis decomposition. In addition, the excellent filtering performance of FRFT has been widely used in noise reduction [2], speech enhancement [3], image processing [4][5], fault detection [6], and other fields. FRFT has good energy aggregation for LFM signals, making it very suitable for their detection, parameter estimation, and separation. A FRFT-based method for separating multiple overlapping LFM signals was proposed in [7]. Although FRFT can achieve optimal matching detection for LFM signals, many shortcomings exist in detecting LFMCW signals. In practice, the receiver can often receive LFMCW signals with multiple periods. However, the gain of FRFT processing is limited to one period, and multiple peaks corresponding to multiple periods are not conducive to signal detection. To solve this problem, the periodic Wigner-Hough transform (PWHT) [8][9] algorithm is proposed in 2010, which achieved complete matching detection of LFMCW signals. However, the disadvantage of WHT is that it is a nonlinear transformation with a large amount of

[1] Henan High-speed Railway Operation and Maintenance Engineering Research Center, China
[2] Henan High-speed Railway Operation and Maintenance Engineering Research Center, China, corresponding author: e-mail: zhujiandong@zzrvtc.edu.cn
[3] Henan High-speed Railway Operation and Maintenance Engineering Research Center, China

computation, which could be more conducive to real-time processing. Zhu [10] and Huang [11] proposed the periodic fractional Fourier transform (PFRFT) algorithm in 2013, which achieved the same detection performance as PWHT while significantly reducing the amount of computation. Zhu [12] further proposed an adaptive threshold estimation method for LFMCW signals based on PFRFT. Nevertheless, they did not consider the PFRFT-based resolution problem of multi-component LFMCW signals. When the peaks of LFMCW signals in the PFRFT domain are too close to be distinguished, it will lead to signal separation failure and target signal leakage.

This article studies the PFRFT-based resolution problem. The spectral characteristics of LFMCW signals in the PFRFT domain are analyzed in Sect 2, and the approximate expression of the energy spectrum of LFMCW signals is derived from discrete PFRFT in Sect 3. Based on analysis of the amplitude superposition of multi-component LFMCW signals, the resolution problem of multi-component LFMCW signals in the PFRFT parameter plane is studied in Sect 4. By selecting a suitable normalization factor of dimension, the resolution ability of PFRFT for multi-component LFMCW signals is improved in Sect 5.

2. The spectral distribution analysis of LFMCW signals in the PFRFT domain

2.1. Review of PFRFT

The PFRFT for signal $x(t)$ is given as follows [10]:

$$PFRFT[x(t)] = \int_{-\infty}^{+\infty} x(t) K_{\tilde{\alpha}}(t,\tilde{\tau},\tilde{u},\tilde{T}) dt \tag{1}$$

The transformation kernel function $K_{\tilde{\alpha}}(t,\tilde{\tau},\tilde{u},\tilde{T})$ is given by

$$K_{\tilde{\alpha}}(t,\tilde{\tau},\tilde{u},\tilde{T}) = \begin{cases} \sqrt{\dfrac{1-j\cot\tilde{\alpha}}{2\pi}} \exp\left(j \dfrac{\mathrm{mod}(t+\tilde{\tau},\tilde{T})^2 + \tilde{u}^2}{2} \cot\tilde{\alpha} \right. \\ \qquad \left. - j(t+\tilde{\tau})\tilde{u}\csc\tilde{\alpha} \right) & \tilde{\alpha} \neq n\pi \\ \sum\limits_{n=-\infty}^{\infty} \delta(t+\tilde{\tau}-\tilde{u}-n\tilde{T}) & \tilde{\alpha} = 2n\pi \\ \sum\limits_{n=-\infty}^{\infty} \delta(t+\tilde{\tau}+\tilde{u}-n\tilde{T}) & \tilde{\alpha} = (2n\pm 1)\pi \end{cases} \tag{2}$$

Where, $\mathrm{mod}(\square)$ denotes the modulus operator. The rotation angle and order of PFRFT are denoted by $\tilde{\alpha} = p\pi/2$ and p respectively, $\tilde{\tau}$ represents the time offset search parameter, while $\tilde{T}$ represents the modulation period (MP) search parameter. Compared with FRFT, the kernel function of PFRFT has two additional parameters $\tilde{T}$ and $\tilde{\tau}$, which can be used to search for unknown parameters and LFMCW signals.

According to Eq. (1), the PFRFT of a signal can also be expressed as:

$$PFRFT[x(t)] = \sum_n \int_0^{\tilde{T}} x(t+n\tilde{T})K(t,\tilde{\tau},\tilde{u})dt \tag{3}$$

This shows that the PFRFT of a signal is actually the result of coherent accumulation in the fractional domain with a period of $\tilde{T}$, which can be used to design a fast implementation algorithm based on FRFT for PFRFT [12].

$$PFRFT[x(t)] = FRFT[\sum_n e^{-j2\pi u(nT-\tau)\csc\alpha} g_T(t-\tau+n\tilde{T})x(t)] \tag{4}$$

Where, g_T is Rectangular window function. A single-component LFMCW signal $s(t)$ can be represented by

$$s(t) = A\exp[j(\varphi + 2\pi f_i t + \pi g \bmod(t+\tau,T)^2)] \tag{5}$$

Where A is the signal amplitude, φ is the random initial phase, f_i is the starting frequency, g is the chirp rate and T is MP of the LFM , τ is the starting time offset, $0 \le \tau < T$, and τ is introduced to consider that the reconnaissance receiver's intercepted signal may not necessarily be at the starting point of the LFM signals.

As mentioned earlier, the PFRFT of LFMCW signals is actually the result of coherent accumulation in the fractional domain with a period of T , so we only analyze one MP of the LFMCW signals here. The thick black line in Fig.1 represents the time-frequency distribution line of one MP of the LFMCW signals, where f_0 is the midpoint of the time-frequency distribution line, and β is the intersection angle between the time axis and the time-frequency distribution direction. The u and v axes are the rotation planes corresponding to the period and time delay (T,τ). $\alpha_0 = p_0\pi/2$ is the optimal rotation angle, and p_0 is the optimal fractional order. A sharp peak is formed by the LFMCW signal at $(\alpha_0, u_{\max}, T, \tau)$, where $u_{\max}$ is the intersection point between the u axis and the time-frequency distribution direction. Therefore, the PFRFT is equivalent to accumulating the signal energy of multiple periods of the LFMCW signal into one period and then performing FRFT.

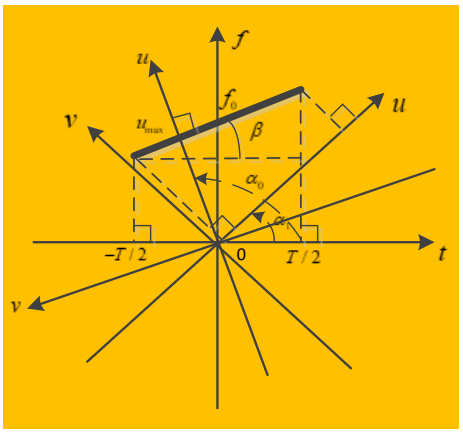

Fig.1. Time frequency distribution of single cycle LFMCW signal

As shown in Fig.1, when $\alpha_0 = \beta + \pi/2$, and $g = \tan\beta$, then $\alpha_0 = arc\cot(-g)$. The projection coordinates u of the midpoint f_0 in the PFRFT domain with a rotation angle α of are given by:

$$u_m = f_0 \sin\alpha \tag{6}$$

Where u_m is the midpoint of u in the PFRFT. When the optimal rotation angle is taken as α_0, the signal spectrum is concentrated at the midpoint to form a peak, and the coordinates of the peak are given by

$$u_{\max} = f_0 \sin\alpha_0$$
$$\sin\alpha_0 = \frac{1}{\sqrt{g^2+1}} \tag{7}$$

We denote ρ as the length of the time-frequency distribution direction in one MP, then $\rho = T/|\cos\beta|$. The intersection angle between the u axis and the time-frequency distribution direction is $\Delta\beta = |\alpha - \beta|$, at rotation angle α. The support width in the PFRFT domain is given by:

$$\rho_\alpha = \left|\frac{T\cos\Delta\beta}{\cos\beta}\right| \tag{8}$$

It can be seen from Eq.7, the variable interval of ρ_α is $[0, \ |T/\cos\beta|]$.

2.2. The Continuous PFRFT Spectral Distribution Characteristics of LFMCW Signals

Assuming the simplified LFMCW signal is

$$s(t) = A\exp(j\pi g \bmod(t+\tau, T)^2) \tag{9}$$

Substituting Eq.(9) into Eq.(1). It can be obtained that

$$PFRFT(\tilde{\alpha},\tilde{u},\tilde{T},\tilde{\tau}) = AA_{\alpha}\int_{-\infty}^{+\infty}\exp[\,j(\pi g \bmod(t+\tau,T)^2 + \frac{\cot\tilde{\alpha}}{2}\bmod(t+\tilde{\tau},\tilde{T})^2) - j\tilde{u}\csc\tilde{\alpha}(t+\tilde{\tau})]dt$$
$$\exp(j\frac{\tilde{u}^2}{2}\cot\tilde{\alpha}) \tag{10}$$

Where, $\tilde{\alpha} \neq n\pi$, $A_{\alpha} = \sqrt{(1-j\cot\tilde{\alpha})/2\pi}$. When $(\tilde{T},\tilde{\tau}) = (T,\tau)$, the PFRFT of the signal at a rotation angle $\tilde{\alpha} = -arc\cot 2\pi g$ is given by

$$\begin{aligned} PFRFT(\tilde{\alpha},\tilde{u},\tilde{T},\tilde{\tau}) &= AA_{\alpha}\exp(j\frac{\tilde{u}^2}{2}\cot\tilde{\alpha})\int_{-\infty}^{+\infty}\exp(-j\tilde{u}\csc\tilde{\alpha}(t+\tilde{\tau}))dt \\ &= AA_{\alpha}\exp(j\frac{\tilde{u}^2}{2}\cot\tilde{\alpha} - j\tilde{u}\tilde{\tau}\csc\tilde{\alpha})\delta(\tilde{u}\csc\tilde{\alpha}) \end{aligned} \tag{11}$$

Which shows that the PFRFT of the signal is an impulse function at the optimal search parameter. In the sampling time, Eq. (11) becomes:

$$PFRFT(\tilde{\alpha},\tilde{u},\tilde{T},\tilde{\tau}) = nAA_{\alpha}T\sin c[\pi T\csc(\tilde{\alpha})\tilde{u}]\exp(j\frac{\tilde{u}^2}{2}\cot\tilde{\alpha} - j\tilde{u}\tilde{\tau}\csc\tilde{\alpha}) \tag{12}$$

Where *n* is the number of MP. It means the optimal PFRFT spectrum follows a Sinc function. When $(\tilde{T},\tilde{\tau}) = (T,\tau)$ and $\tilde{\alpha} \neq -arc\cot 2\pi g$, Eq.(12) can be transformed as

$$\begin{aligned} PFRFT(\tilde{\alpha},\tilde{u},\tilde{T},\tilde{\tau}) &= nAA_{\alpha}\exp[\,j\frac{\tilde{u}^2}{2}(\cot\tilde{\alpha} - \frac{\csc^2\tilde{\alpha}}{2\pi g+\cot\tilde{\alpha}})] \\ &\int_{-T/2}^{T/2}\exp[\,j\frac{\pi}{2}(2g+\frac{\cot\tilde{\alpha}}{\pi})(t+\tau-\frac{\tilde{u}\csc\tilde{\alpha}}{2\pi g+\cot\tilde{\alpha}})^2]dt \end{aligned} \tag{13}$$

Assuming $2g+\cot\tilde{\alpha}/\pi > 0$, and $z = \sqrt{2g+\frac{\cot\tilde{\alpha}}{\pi}}(t+\tau-\frac{\tilde{u}\csc\tilde{\alpha}}{2\pi g+\cot\tilde{\alpha}})$, then

$$PFRFT(\tilde{\alpha},\tilde{u},\tilde{T},\tilde{\tau}) = \frac{nAA_{\alpha}}{\sqrt{2g+\frac{\cot\tilde{\alpha}}{\pi}}}\exp[\,j\frac{\tilde{u}^2}{2}(\cot\tilde{\alpha} - \frac{\csc^2\tilde{\alpha}}{2\pi g+\cot\tilde{\alpha}})]\int_{-T_1}^{T_2}\exp(j\frac{\pi}{2}z^2)dz \tag{14}$$

Where,

$$-T_1 = \sqrt{2g+\cot\tilde{\alpha}/\pi}(-T/2+\tau-\tilde{u}\csc\tilde{\alpha}/(2\pi g+\cot\tilde{\alpha})) \tag{15}$$

$$T_2 = \sqrt{2g+\cot\tilde{\alpha}/\pi}(T/2+\tau-\tilde{u}\csc\tilde{\alpha}/(2\pi g+\cot\tilde{\alpha}))\,. \tag{16}$$

The PFRFT spectrum expression of a finite-length LFMCW signal is

$$\begin{aligned} PFRFT(\tilde{\alpha},\tilde{u},\tilde{T},\tilde{\tau}) &= \frac{nAA_{\alpha}}{\sqrt{2g+\frac{\cot\tilde{\alpha}}{\pi}}}\{[c(T_1)+c(T_2)] + j[s(T_1)+s(T_2)]\} \\ &\exp[\,j\frac{\tilde{u}^2}{2}(\cot\tilde{\alpha} - \frac{\csc^2\tilde{\alpha}}{2\pi g+\cot\tilde{\alpha}})] \\ &= \frac{nAA_{\alpha}}{\sqrt{2g+\frac{\cot\tilde{\alpha}}{\pi}}}\{[c(T_1)+c(T_2)]^2 + [s(T_1)+s(T_2)]^2\}^{1/2} \\ &\exp\{j[\arctan\frac{s(T_1)+s(T_2)}{c(T_1)+c(T_2)} + \frac{\tilde{u}^2}{2}(\cot\tilde{\alpha} - \frac{\csc^2\tilde{\alpha}}{2\pi g+\cot\tilde{\alpha}})]\} \end{aligned} \tag{17}$$

Here, $c(T)=\int_0^T \cos(\frac{\pi}{2}z^2)dz$, $s(T)=\int_0^T \sin(\frac{\pi}{2}z^2)dz$ denotes the Fresnel integral function, obtains:

$$\begin{aligned}\left|PFRFT(\tilde{\alpha},\tilde{u},\tilde{T},\tilde{\tau})\right| &= \frac{nAA_\alpha}{\sqrt{2g+\frac{\cot\tilde{\alpha}}{\pi}}}\{[c(T_1)+c(T_2)]^2+[s(T_1)+s(T_2)]^2\}^{1/2} \\ \theta(\tilde{\alpha},\tilde{u},\tilde{T},\tilde{\tau}) &= \arctan\frac{s(T_1)+s(T_2)}{c(T_1)+c(T_2)}+\frac{\tilde{u}^2}{2}(\cot\tilde{\alpha}-\frac{\csc^2\tilde{\alpha}}{2\pi g+\cot\tilde{\alpha}})\end{aligned} \tag{18}$$

When $\tilde{u}=0$, $T_1=\sqrt{2g+\cot\tilde{\alpha}/\pi}(T/2-\tau)$, $T_2=\sqrt{2g+\cot\tilde{\alpha}/\pi}(T/2+\tau)$, and when $\sqrt{2g+\cot\tilde{\alpha}/\pi}$ □ 1 , the Fresnel integral function, $c(T)=s(T)\approx 0.5$,which can be substituted into Eq. (18) to obtain:

$$\left|PFRFT(\tilde{\alpha},0,\tilde{T},\tilde{\tau})\right| = nAA_\alpha/\sqrt{g+\frac{\cot\tilde{\alpha}}{2\pi}}\ ,\ \arctan\frac{s(T_1)+s(T_2)}{c(T_1)+c(T_2)}\approx\frac{\pi}{4} \tag{19}$$

when $\tilde{u}=-\rho_\alpha/2$, $T_1=-\tau\sqrt{2g+\cot\tilde{\alpha}/\pi}$, $T_2=(T+\tau)\sqrt{2g+\cot\tilde{\alpha}/\pi}$, and when $\tau=0$, obtains $T_1=0$, $T_2=T\sqrt{2g+\cot\tilde{\alpha}/\pi}$; when $\tilde{u}=\rho_\alpha/2$, $T_1=T\sqrt{2g+\cot\tilde{\alpha}/\pi}$, $T_2=0$. Substituting T_1 and T_2 into Eq. (18) obtains:

$$\left|PFRFT(\tilde{\alpha},\pm\rho_\alpha/2,\tilde{T},0)\right| = nAA_\alpha/(2\sqrt{g+\frac{\cot\tilde{\alpha}}{2\pi}}) \tag{20}$$

The amplitude value is half of when $\tilde{u}=0$. As $\sqrt{2g+\cot\tilde{\alpha}/\pi}$ increases, the reduced fluctuation of the Fresnel integral function value in the support interval $u\in(-\rho_\alpha/2,\rho_\alpha/2)$ means that the PFRFT spectrum of the signal is flat. Thus, the spectrum shape is closer to a rectangle. Fig.2 shows a three-dimensional slice of the PFRFT domain spectrum of an LFMCW signal when $(\tilde{T},\tilde{\tau})=(T,\tau)$.

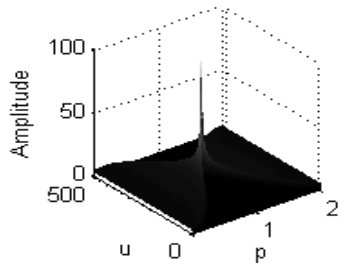

Fig. 2. 3D Spectrum Distribution of LFMCW Signal in PFRFT Domain

3. Discrete PFRFT Spectral Characteristics of LFMCW Signal

3.1. Influence of Dimensional Normalization on the Periodic Fractional Fourier Spectrum of LFMCW Signals

In practical applications, digital signal processing of PFRFT is generally used. Ozaktas [13] proposed a fast discrete FRFT algorithm, one of the most commonly used algorithms due to its high accuracy and low complexity. The

PFRFT is equivalent to the coherent accumulation of the FRFT of each period of the LFM signal, so the discrete algorithm for PFRFT is based on the discrete FRFT algorithm with the same processing of dimensional normalization. The dimensional normalization method is as follows: assuming that the original signal is tightly supported on both the time and frequency axes, the time domain interval is $[-\Delta t/2,\ \Delta t/2]$ and the frequency domain interval is $[-\Delta f/2,\ \Delta f/2]$,which have different dimensions. To facilitate calculation and processing, both the time and frequency domains need to be transformed into a unified dimension. Introduce the dimensional normalization factor $s=(\Delta t/\Delta f)^{1/2}$ and define the dimensional normalization coordinates as $x=t/s$, $v=fs$. The new coordinate (x,v) system achieves dimensional normalization.

In practical applications, only the discrete data obtained by sampling the original continuous signal can be obtained. This paper adopts the discrete scaling method as follows [14] : let the time width of the signal be $\Delta t=T_d$, the bandwidth be $\Delta f=f_s$, then $s=(T_d/f_s)^{1/2}$. The time domain and frequency domain intervals of the signal become $[-\Delta x/2,\ \Delta x/2]$, where $\Delta x=(T_d f_s)^{1/2}$. The new coordinate system achieves dimensional normalization, and the sampling interval becomes $1/\Delta x$.

Assuming that the new chirp rate after dimensional normalization is g' , the initial frequency is f_i' , the corresponding optimal rotation angle is $\hat{\alpha}_0$, and the coordinates of the maximum value are $\hat{u}_{\max}$. The quantization relationship between them is

$$\begin{cases} g'=-\cot\hat{\alpha}_0/(2\pi) \\ f_i'=\hat{u}_{\max}\csc\hat{\alpha}_0/(2\pi) \end{cases} \tag{21}$$

According to [14], the actual parameter values after dimensional normalized are:

$$\begin{cases} g'=v/x=(fs)/(t/s)=gT_d/f_s \\ f_i'=f_i s=f_i(T_d/f_s)^{1/2} \end{cases} \tag{22}$$

Combining the above two equations, the peak coordinates can be obtained as:

$$\begin{cases} \hat{\alpha}_0=arc\cot(-2\pi gT_d/f_s) \\ \hat{u}_{\max}=2\pi f_i(T_d/f_s)^{1/2}\sin\hat{\alpha}_0 \end{cases} \tag{23}$$

Eq. (23) shows that dimensional normalization changes the coordinates of the signal peak. The support area width in the PFRFT domain and the coordinates of the midpoint are changed as follows, respectively:

$$\begin{aligned} \rho_\alpha' &= \left|\frac{\Delta x\cos\Delta\beta}{n\cos\beta}\right|=\left|\frac{\Delta x}{n}(\cos\alpha+gT_d/f_s\sin\alpha)\right| \\ u_m' &= f_i\sqrt{T_d/f_s}\sin\alpha \end{aligned} \tag{24}$$

Where n is the number of frequency modulation cycles.

3.2 Approximate Expression of Discrete PFRFT Spectrum for LFMCW Signal

For the continuous signal in Eq. (9), according to Eq. (12), when $\tilde{u}=0$, the spectrum maximum value of $s(t)$ in the optimal PFRFT domain is

$$\left|PFRFT(\tilde{\alpha},0,\tilde{T},\tilde{\tau})\right|=\left|nAA_{\alpha}T\right|=\frac{\left|nAT\right|}{\left|2\pi\sin\tilde{\alpha}_0\right|^{1/2}} \tag{25}$$

After the continuous signal $s(t)$ is sampled and dimensionally normalized, the maximum value of the spectrum becomes

$$\left|PFRFT(\tilde{\alpha},0,\tilde{T},\tilde{\tau})\right|=\frac{\left|A\right|(2N+1)}{2\sqrt{N}\left|2\pi\sin\tilde{\alpha}_0\right|^{1/2}}\approx\frac{\left|A\right|\sqrt{N}}{\left|2\pi\sin\tilde{\alpha}_0\right|^{1/2}}=\frac{\left|A\right|\Delta x}{\left|2\pi\sin\tilde{\alpha}_0\right|^{1/2}} \tag{26}$$

Comparing Eq. (26) with Eq. (25), it can be seen that the maximum value of the PFRFT-spectrum changes after dimensional normalization. The modulus squared maximum is

$$\left|PFRFT(\tilde{\alpha},0,\tilde{T},\tilde{\tau})\right|^2_{\max}=\frac{\left|A\right|^2N}{\left|2\pi\sin\tilde{\alpha}_0\right|} \tag{27}$$

Eq. (24) gives the support width of the signal in the PFRFT domain after dimensional normalization, and the sampling interval of the signal is $1/\Delta x$. Then, the sampling points number in the support area is

$$N_{\rho\alpha}=\mathrm{int}eger(\rho'_{\alpha}/\frac{1}{\Delta x})+1=\mathrm{int}eger[\left|\frac{N}{n}(\cos\alpha+gT_d/f_s\sin\alpha)\right|]+1 \tag{28}$$

Where $\mathrm{int}eger(\square)$ represents the integer part of an actual number. Further derivation shows that the approximate expression of the energy spectrum is

$$\left|PFRFT(\tilde{\alpha},\tilde{u},\tilde{T},\tilde{\tau})\right|^2=\begin{cases}\dfrac{\left|A\right|^2N}{\left\{\mathrm{int}eger[\left|\frac{N}{n}(\cos\alpha+gT_d/f_s\sin\alpha)\right|]+1\right\}\left|2\pi\sin\tilde{\alpha}_0\right|}, & \\ \qquad\qquad \tilde{u}\in[u'_m-\dfrac{\rho'_{\alpha}}{2},u'_m+\dfrac{\rho'_{\alpha}}{2}] & \\ 0 \qquad\qquad , \quad \tilde{u}\notin[u'_m-\dfrac{\rho'_{\alpha}}{2},u'_m+\dfrac{\rho'_{\alpha}}{2}] & \end{cases} \tag{29}$$

4. Resolution analysis of multi-component LFMCW signals

Multi-component LFMCW signals can be represented as

$$x(t)=\sum_{m=1}^{M}A_m\exp[j(2\pi f_m t+\pi g_m(\mathrm{mod}(t+\tau_m,T_m))^2+\varphi_m)], \quad -T_d/2\le t\le T_d/2 \tag{30}$$

Where M is the number of signal components. Multi-component LFMCW signals with similar energy and parameters may appear indistinguishable due to the

superposition of energy spectra in the PFRFT domain, resulting in missed detections. This section uses the PFRFT distribution characteristics of LFMCW signals in Sections 2 and 3 to analyze the resolution problem between multi-component LFMCW signals quantitatively. When $(\tilde{T},\tilde{\tau})=(T,\tau)$ is fixed, the resolution of two LFMCW signals in the parameter plane $(p,\tilde{u})$ includes the resolution on the axis and the axis. If the signals can be resolved on one axis, then the two signals can be distinguished. The signals cannot be distinguished if they cannot be resolved on both axes.

Take two LFMCW signals s_r and s_l, with initial frequencies f_r and f_l, and chirp rate g_r and g_l, respectively. Assume that their best rotation angles are α_r and α_l ($\alpha_r = p_r\pi/2,\ \alpha_l = p_l\pi/2$, assume $\alpha_r < \alpha_l$); the axis coordinates of the maximum energy spectrum points in their respective optimal period FRFT domain are $\tilde{u}'_{r\max}$ and $\tilde{u}'_{l\max}$, respectively; and the coordinates of their peaks in the plane $(p,\tilde{u})$ are $(p_r,\tilde{u}'_{r\max})$ and $(p_l,\tilde{u}'_{l\max})$, respectively. Let $\tilde{u}'_{rm}$ and $\tilde{u}'_{lm}$ be the midpoints of s_r and s_l in each PFRFT spectra, respectively; and let $\rho'_{r\alpha}$ and $\rho'_{l\alpha}$ be the widths of their PFRFT spectra, respectively. The distances between their peaks on the and axes are ΔR_p and ΔR_u, respectively. According to Eq. (26) and (27), it can be seen that in the PFRFT domain with a rotation angle of α_r, the energy of signal is mainly concentrated at one point $\tilde{u}'_{r\max}$, and the value is $|A_r|^2 N/|2\pi\sin\alpha_r|$. Furthermore, according to Eq. (12), the PFRFT distribution of s_r is a sinc function $\sin c[\pi T\csc(\alpha_r)\tilde{u}]$, and becomes $\sin c[\pi\frac{\Delta x}{n}\csc(\alpha_r)\tilde{u}]$ after Dimensional normalization, with the support region width of $\frac{2n}{\Delta x\csc(\alpha_r)}$, which is approximately chosen as $\frac{2n}{\Delta x}$. Similarly, in the rotation angle of α_l. The critical resolution distances of s_r and s_l on the p and $\tilde{u}$ axis are analyzed below.

There are two cases to consider: (1) the support regions of s_r and s_l do not overlap, which needs $|\tilde{u}'_{rm}-\tilde{u}'_{lm}|>(\rho'_{r\alpha}+\rho'_{l\alpha})/2$, when $\alpha\in[\alpha_r,\alpha_l]$; (2) the support regions of s_r and s_l overlap, which needs $|\tilde{u}'_{rm}-\tilde{u}'_{lm}|\le(\rho'_{r\alpha}+\rho'_{l\alpha})/2$, when $\alpha\in[\alpha_r,\alpha_l]$.

For the first case, there is no significant amplitude difference between the two peaks on the axis p, the two signals cannot be distinguished. According to Eq. (24), when $|\frac{N}{n}(\cos\alpha+gT_d/f_s\sin\alpha)|<1$, the energy spectrum amplitude of the signal is similar to the maximum value. Let the interval of α that satisfies this inequality be $\Delta\alpha$, and the peak of the signal cannot be highlighted in this α interval. Taking s_r as an example, it can be analyzed which factors are related to $\Delta\alpha_r$ from $|\frac{N}{n}(\cos\alpha+gT_d/f_s\sin\alpha)|=|\frac{T_d}{n}\sqrt{f_s^2+g_r^2T_d^2}\sin(\alpha_r-\alpha)|<1$.

It can be obtained that:

$$\Delta\alpha_r = 2\arcsin(\frac{n}{T_d\sqrt{f_s^2 + g_r^2 T_d^2}}) \tag{31}$$

According to Eq. (31), The influencing factors of width $\Delta\alpha_r$ includes the chirp rate g_r, the sampling time T_d, the sampling frequency f_s, and the MP number n, and the midpoint of the interval is α_r. Based on the above analysis, the critical resolution distance of s_r and s_l on the axis p in the first case is

$$\Delta R_{p\min 1} = \frac{1}{2}(\Delta\alpha_r + \Delta\alpha_l)/(\pi/2) \tag{32}$$

When $\Delta R_p \le \Delta R_{p\min 1}$, s_r and s_l cannot be distinguished on the axis p.

For the second case, the support regions of s_r and s_l overlap, and the effect of energy spectrum superposition on signal resolution needs to be considered. Taking the typical case $f_r = f_l$, the support regions of s_r and s_l overlap in any PFRFT domain. According to Eq. (29), when $1 \le |\frac{N}{n}(\cos\alpha + gT_d / f_s \sin\alpha)| < 2$, the superposition value of the energy spectrum of s_r and s_l is similar to the maximum energy spectrum amplitude in the FRFT domain of α_r and α_l. Thus, in the interval that satisfies this condition, the peaks of the two signals cannot be distinguished. When $|\frac{N}{n}(\cos\alpha + gT_d / f_s \sin\alpha)| > 2$ the energy spectrum's superposition value is much larger than the peak value difference, the signals can be distinguished. Therefore, the critical resolution distance of the second case is

$$\begin{aligned}\Delta R_{p\min 2} = \{&\frac{1}{2}(\Delta\alpha_r + \Delta\alpha_l) + \min[\arcsin(\frac{2n}{T_d\sqrt{f_s^2 + g_r^2 T_d^2}}) - \frac{\Delta\alpha_r}{2},\\ &\arcsin(\frac{2n}{T_d\sqrt{f_s^2 + g_r^2 T_d^2}}) - \frac{\Delta\alpha_l}{2}]\}/(\pi/2)\\ =[&\frac{\Delta\alpha_r}{2} + \arcsin(\frac{2n}{T_d\sqrt{f_s^2 + g_r^2 T_d^2}})]/(\pi/2)\end{aligned} \tag{33}$$

Where $\min(\square)$ represents the smaller of the two data (it is assumed above that $\alpha_r < \alpha_l$). When $\Delta R_p \le \Delta R_{p\min 2}$, s_r and s_l cannot be distinguished on the axis p.

In the above two cases, the critical resolution distance analysis on the axis $\tilde{u}$ is as follows. In the first instance, when $|\tilde{u}'_{rm} - \tilde{u}'_{lm}| > (\rho'_{r\alpha} + \rho'_{l\alpha})/2$, the peak of s_r is not in the support region of s_l, and s_r and s_l have little influence on each other, and can be differentiated on the axis $\tilde{u}$. In the second instance, when $|\tilde{u}'_{rm} - \tilde{u}'_{lm}| \le (\rho'_{r\alpha} + \rho'_{l\alpha})/2$ and $|p_l - p_r| < \Delta R_{p\min 2}$, the peak distance between s_r and s_l on the axis $\tilde{u}$ is less than $4n$ the sampling interval $4n/\Delta x$, so the energy superposition effect of s_r and s_l leads to indistinguishability of their peak on the axis $\tilde{u}$. When the peak distance between s_r and s_l on the axis $\tilde{u}$ is larger than $4n$ the sampling interval $4n/\Delta x$, and the energy spectrum of s_r and s_l does not overlap

on the axis $\tilde{u}$, and can be differentiated on the axis $\tilde{u}$. Therefore, in the second instance, the critical resolution distance of s_r and s_l on the axis $\tilde{u}$ is:

$$\Delta R_{u\min} = \frac{4n}{\sqrt{T_d f_s}} \tag{34}$$

It can be concluded that:(a)when the peaks distance between the signals s_r and s_l, satisfies $\Delta R_p < \Delta R_{p\min 2}$, and $\Delta R_u < 4n/\Delta x$, the peaks cannot be distinguished; (b)the critical resolution distance between signals s_r and s_l is not only related to the parameters of the signal, but also affected by the Dimensional normalization under the condition of discrete PFRFT calculation.

5. Selection of Dimensional Normalization Factor

From Eq.(23), it can be seen that under the condition of discrete PFRFT calculation, the distance between the peak of s_r and s_l on the axis p is

$$\Delta R_p = |p_l - p_r| = |arc\cot(-2\pi g_l T_d / f_s) - arc\cot(-2\pi g_r T_d / f_s)| / (\pi/2) \tag{35}$$

and the distance on the axis $\tilde{u}$ is

$$\begin{aligned} \Delta R_u &= |u_{r\max} - u_{l\max}| \\ &= (T_d / f_s)^{1/2} |f_l \sin\alpha_l - f_r \sin\alpha_r| \\ &= (T_d / f_s)^{1/2} \left| \frac{f_l}{\sqrt{1 + g_l^2 (T_d / f_s)^2}} - \frac{f_r}{\sqrt{1 + g_r^2 (T_d / f_s)^2}} \right| \end{aligned} \tag{36}$$

From Eq. (35) and (36), it can be observed that the distance between signal peaks is regulated by the dimensionality normalization factor $s = (T_d / f_s)^{1/2}$. Obviously, as long as the sampling theorem is satisfied, optimizing the Dimensional normalization factor increases the peak distance on the parameter plane $(p, \tilde{u})$. When ΔR is maximum, the resolution is optimal, that is,

$$\Delta R_{\max} = \max(\sqrt{\Delta R_p^2 + \Delta R_u^2}) \tag{37}$$

Therefore, when two signals cannot be distinguished, a reasonable Dimensional normalization factor can be selected to make ΔR as large as possible and achieve their resolution.

Taking two sets of parameters as examples, the variation of peak distance between two signals with the factor s is analyzed bellow. (1) When $f_r = 20Hz$, $f_l = 22Hz$, and $g_r = 20Hz/s$, $g_l = 24Hz/s$; (2) When $f_r = 200Hz$, $f_l = 220Hz$, $g_r = 1500Hz/s$ and $g_l = 1600Hz/s$, ΔR_p and ΔR_u change with $s = (T_d / f_s)^{1/2}$ as shown in the curves in Fig.3.

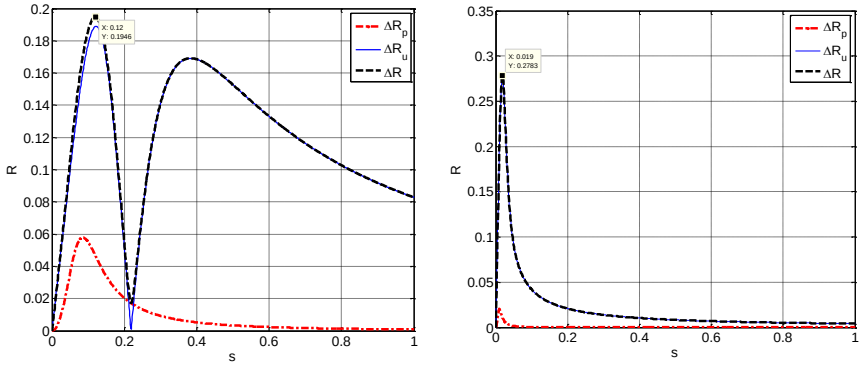

(a) (b)

Fig. 3. Variation curves of three kind of peaks distance of two signal with the change of s. (a)fr=20Hz, fl=22Hz, gr=20Hz/s, gl=24Hz/s, (b) fr=200Hz, fl=220Hz, gr=1500Hz/s, gl=1600Hz/s.

From Fig. 3, it can be seen that: (a)Both the peaks distance of the two LFMCW signal on the u-axis and p-axis is regulated by s, and get maximum values at different s; (b) the the peaks distance adjustment of the two signal on the u-axis is much larger than that on the p-axis, so the position where ΔR reaches the maximum value mainly depends on the coordinate of the maximum value of ΔR_{u}, for the first and second sets of data, when s=0.12 and 0.019, respectively.

Taking the first set of data above as an example, the amplitude of the two signals is set to 1 to verify the selection of the Dimensional normalization factor to achieve the resolution of the two LFMCW signals. For the first set of data: when $T_d = 4s$, $f_s = 1000Hz$, and $n = 4$, the three-dimensional distribution slice of the two signals at $(T = 1, \tau = 0)$ is shown in Fig. 4. When $T_d = 4s$, $f_s = 278Hz$, and $n = 4$, $s = (T_d / f_s)^{1/2} = 0.12$, the three-dimensional distribution slice of the two signals at $(T = 1, \tau = 0)$ is shown in Fig.5.

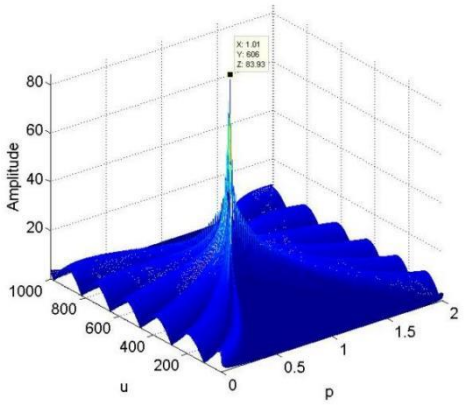

Fig. 4. The 3D-slice PFRFT of the signals, s=0.0632

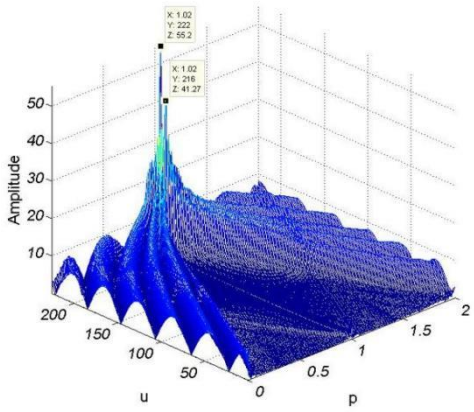

Fig. 5. The 3D-slice PFRFT of the signals, s=0.12

It can be seen that in Fig. 4, the two signals are mixed together and cannot be distinguished, while in Fig. 5, the two signals can be distinguished by increasing the Dimensional normalization factor s to increase the two peaks distance, which verifies the rationality of determining the optimal normalization factor based on Eq. (37) and the peak distance change curve in Fig. 3. As mentioned earlier, the critical resolution distance between two LFMCW signals is related to two kinds of elements, the signal parameters and Dimensional normalization factor. Since the parameters of signals are uncontrollable, and this paper adopts a Dimensional normalization factor of $s=(T_d / f_s)^{1/2}$, reasonable sampling time T_d and sampling frequency f_s can be selected under the condition of satisfying the sampling theorem to improve the resolution of the PFRFT.

6. Conclusion

This paper analyzes the frequency spectrum distribution characteristics of LFMCW continuous and discrete signals in the PFRFT domain and derives an approximate expression for the energy spectrum of LFMCW signals under discrete PFRFT calculation. Based on the analysis of the resolution distance on the PFRFT parameter plane, the resolution problem of multiple LFMCW signals was investigated. Research found that the resolution distance is related to the following factors: (1) signal parameters: initial frequency, chirp rate, frequency modulation cycle, observation time, sampling frequency; (2) Dimensional normalization factor. The resolution capability of PFRFT to multiple LFMCW signals can be improved.

REFERENCES

[1] *Qi L, Tao R, Zhou S Y, et al*., Detection and parameter estimation of multicomponent LFM signals based on the fractional Fourier transform. Science in China Series F: Information Sciences, 2004, 47(2): 184-198.

[2] *M. Alper Kutay, Haldun M. Ozaktas, Levent Onural*. Optimal filtering in fractional fourier domain. IEEE Transactions on Signal Processing, 1997,45(5): 1129-1143.

[3] *Kunche, P., Manikanthababu, N.*, Dual Channel Speech Enhancement Based on Fractional Fourier Transform. In: Fractional Fourier Transform Techniques for Speech Enhancement. Springer Briefs in Speech Technology. Springer, Cham, pp 51–70, 2020.

[4] *Cuneyd Ozturk and Haldun M. Ozaktas and Sinan Gezici and Aykut Koç*, Optimal Fractional Fourier Filtering for Graph Signals. IEEE Transactions on Signal Processing, 69, 2902-2912, 2021.

[5] *Wang, Y., Peng, Z., Han, Y.et al*., Seismic Attribute Analysis with Saliency Detection in Fractional Fourier Transform Domain. J. Earth Sci. 2018, 29, 1372–1379.

[6] *Chen G, Yan C, Meng J, et al*., Improved VMD-FRFT based on initial center frequency for early fault diagnosis of rolling element bearing. Measurement Science and Technology, 2021, 32(11):115-124.

[7] *Cowell D M J*, Freear S. Separation of overlapping linear frequency modulated(LFM) signals using the fractional Fourier transform. IEEE Transactions on Ultrasonics, Ferroelectrics and Frequency Control, 2010, 57(10): 2324-2333.

[8] *Geroleo F G and Pearce M B*., Detection and estimation of multipulse LFMCW radar signals. 2010 IEEE International Radar Conference, Arlington, 2010: 1009-1013.

[9] *Geroleo F G and Pearce M B*., Detection and estimation of LFMCW radar signals. IEEE Transactions on Aerospace and Electronic Systems, 2012, 48(1): 405-417.

[10] *Zhu J D, Zhao Y J, Tang J*., Periodic FRFT Based Detection and Estimation for LFMCW Radar Signal separating. Journal of Electronics and Information Technology, 2013, 35(8): 1827-1833.

[11] *Huang Y, Liu F, Wang Z Z,*. Periodic FRFT-Based Multi-component LFMCW Radar Signal separation.Acta Aeronautica and Astronautica Sinica, 2013, 34(4): 846-854.

[12] *Jiandong Zhu, Jinliang Li, Xiangdong Gao,Libang Ye, Huanyao Dai*., Adaptive Threshold Detection and Estimation of Linear Frequency-Modulated Continuous-Wave Signals Based on Periodic Fractional Fourier Transform. Circuits, Systems, and Signal Processing, 2016, 35(7): 2502-2517.

[13] *Haldun M. Ozaktas, M. Arikan O*, Alper Kutay, et al. Digital computation of the fractional Fourier transform. IEEE Trans Signal Proces, 1996, 44(9): 2141-2150.

[14] *Zhao X H, Deng B, Tao R*., Dimensional Normalization in the Digital Computation of the Fractional Fourier Transform. Transactions of Beijing Institute of Technology, 2005, 25(4): 360-364.